DEFECT ASSESSMENT ON PIPE USED FOR TRANSPORT OF MIXTURE OF HYDROGEN AND NATURAL GAS

Capelle, J.[1], Gilgert, J.[1] and Pluvinage, G.[1]
[1] Laboratoire de mécanique Biomécanique Polymère Structure (LaBPS),
Ecole Nationale d'Ingénieurs de Metz (ENIM),
Ile du Saulcy, Metz, 57045, France, capelle@enim.fr

ABSTRACT

The present article indicates the change of mechanical properties of X52 gas pipe steel in presence of hydrogen and its consequence on defect assessment particularly on notch like defects. The purpose of this work is to determine if the transport of a mixture of natural gas and hydrogen in the actual existing European natural gas pipe network can be done with a reasonable low failure risk (i.e. a probability of failure less than 10^{-6}). To evaluate this risk, a deterministic defect assessment method has been established. This method is based on Failure Assessment Diagram and more precisely on a Modified Notch Failure Assessment Diagram (MNFAD) which has been proposed for this work. This MNFAD is coupled with the SINTAP failure curve and allows determining the safety factor associated with defect geometry, loading conditions and material resistance. The work described in this paper was performed within the NATURALHY work package 3 on 'Durability of pipeline material'.

1.0 INTRODUCTION

1.1 European Gas Network

The European gas pipelines network plays very important role for national economies as well as global. This importance will permanently increase with prospective plans of introducing of European hydrogen energy infrastructure [1, 2] and the possible use of existing pipeline networks for transportation of natural gas and hydrogen mixtures. Within the European project NATURALHY [3], 39 European partners have combined their efforts to assess the effects of the presence of hydrogen on the existing gas network. Key issues are durability of pipeline material, integrity management, safety aspects, life cycle and socio-economic assessment and end-use. The work described in this paper was performed within the NATURALHY work package 'Durability of pipeline material'. The causes of the failures of the gas pipelines are various natures, Fig. 1. They can appear either by fracture, or by leak (it depends of the nature of the fluid transported). The majority of these failures are caused by pitting corrosion or cracking by stress corrosion, but there are also problems related to weld defects. Movements of ground (landslip, earthquake ...) can also be the cause of damage on the buried pipelines. The owners of pipelines study these problems for a long time and have a good knowledge of the methods allowing managing them.

External mechanical aggressions are the cause of many problems, Fig. 1. Indeed, it happens that pipelines are damaged or perforated accidentally at time of excavation work. Crack initiation in and rupture emanating from stress concentrations are at origin of more than 90% of service failures. The presence of a geometrical discontinuity such as a notch will cause weakening of the fracture resistance of the pipeline, reduce the cross section of the pipe, making it more sensitive to the operating pressure and loads caused by soil movements. In this paper, authors are developed a new tool based on Failure Assessment Diagram, Structural INTegrity Assessment Procedure for european industry (SINTAP), and the Volumetric Method. This tool allows to assess the nocivity of a notch type defect, in using two different factors: the security factor and the safety factor.

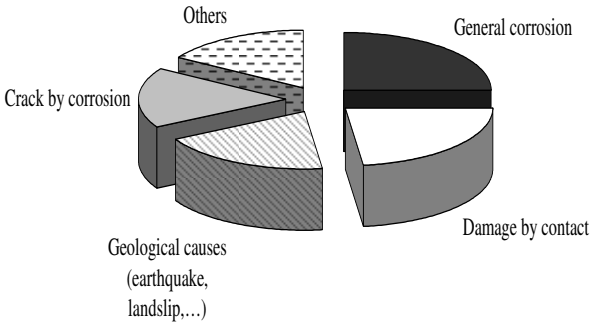

Figure 1. Causes of the fracture of pipelines in the course of exploitation recorded by the members of the ACPRÉ of 1985 to 1995 [4]

1.2 Steel used

The studied steel, API 5L X52, is traditionally for pipelines manufacturing. This steel was the most common gas pipelines material for transmission of oil and gas during 1950-1960. The standard chemical composition and mechanical properties of this steel are shown in tables 1 and 2.

Table 1. Chemical composition of the steel (mass proportion in %).

C	Mn	Si	Cr	Ni	Mo	S	Cu	Ti	Nb	Al
0.116	1.286	0.226	0.055	0.033	0.011	0.001	0.024	0.003	<0.02	0.034

Table 2. Mechanical properties of API X52 [5].

E (GPa)	σ_Y (MPa)	σ_U (MPa)	A%	n	K (MPa)
203	453	524	14	0.0446	587.3

Where E, σ_Y, σ_U, A%, n, and K are respectively the Young's modulus, yield stress, ultimate stress, ultimate elongation, hardening exponent, and hardening coefficient. The material stress strain behaviour is described by the Ludwik's law [5] according to:

$$\sigma = K\varepsilon_p^n \tag{1}$$

2.0 DEFECT ASSESSMENT

2.1 Failure Assessment Diagram and SINTAP

In this study, we chose to use a deterministic approach, derive from SINTAP procedure and Failure Assessment Diagram (FAD). The SINTAP procedure is based on the principle of fracture mechanics and limit analysis, it is used to assess defects in structures, known or assumed. Philosophy of this approach is reflected in the fact that data quality is reflected in the sophistication and accuracy of results. To do this, there are several levels of analysis, more and more complex by allowing the data to obtain a specific result. The lowest level provides the most conservative. All failure in elasto-plastic is characterized by a point in a diagram named Failure Assessment Diagram. This diagram accounts any kinds of failure: plastic collapse as well as brittle fracture and elastic-plastic failure, Fig. 2. The FAD

exhibits a failure curve as the critical non dimensional stress intensity factor versus non dimensional stress or loading parameter and has been applied into several codes in conjunction with the structural integrity of cracked structures. The interpolation between two limits states, is obtained by a curve representing the fracture limit, called Failure Integrity Line. Many interpolation curves have been proposed. We have chosen to use the curve given by the SINTAP procedure. The mathematical expressions of SINTAP default level procedure with the aforementioned assumption can be written as below [6]:

$$f(L_r) = \left[1 + \frac{L_r^2}{2}\right]^{\frac{-1}{2}} \left[0.3 + 0.7 \times e^{\left(-0.6 \times L_r^2\right)}\right], \quad \text{for } 0 \le L_r \le 1 \text{ where } L_r^{max} = 1 + \left(\frac{150}{\sigma_Y}\right)^{2.5}, \tag{2}$$

wherein $f_{(Lr)}$, L_r, L_r^{max} and σ_Y are respectively interpolating function, non dimensional loading or stress based parameter, the maximum value of non dimensional loading or stress based parameter and yield stress, respectively.

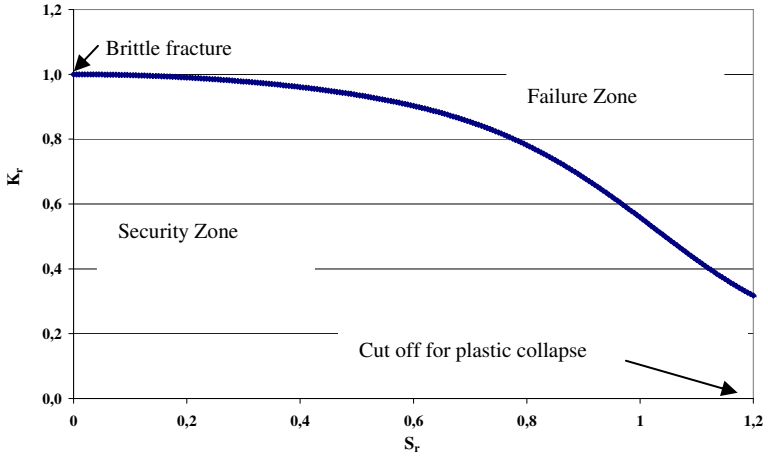

Figure 2. Failure Assessment Diagram

The FAD, parameters are defined as follows:

Non dimensional stress
$$S_r = \frac{\sigma_g}{\sigma_y}, \tag{3}$$

Non dimensional applied stress intensity factor
$$K_r = \frac{K_I}{K_{IC}}, \tag{4}$$

where σ_g, σ_y, K_I and K_{IC} are: gross stress, yield stress, stress intensity factor and critical stress intensity factor.

Point A, on the Fig. 3 is the assessment point obtained after calculation of the two parameters, K_r and S_r. To have the safety factor based on the size of the defect, we need to know two other points, O, origin point of the diagram, and D, point corresponding to the intersection between the Failure Integrity Line and straight line (OA). The value of the safety factor is given by the ratio:

$$f_{s,a} = \frac{OD}{OA}, \tag{5}$$

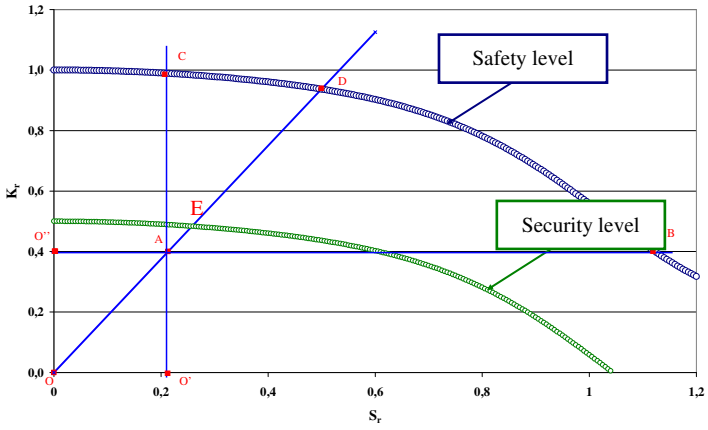

Figure 3. Security factor in a Failure Assessment Diagram

In the same way, we can obtain the security factor, it is only necessary to replace the point D, by the point E, intersection between the Security Level Line and straight (OA).

2.2 Modified Notch Failure Assessment Diagram

The SINTAP procedure introduced previously is only available for one type of defect: cracks. However, the goal of our study concerns the characterization of defects obtained by external interferences. These defects are considered like notches. We have therefore decided to adapt this procedure to our needs, and to use a Modified Notch Failure Assessment Diagram (MNFAD). The news parameters of the MFAD are the following:

$$K_{\rho,r} = \frac{K_{\rho,app}}{K_{\rho,c}}, \tag{6}$$

$$S_r = \frac{\sigma_{\theta\theta}}{\sigma_0}, \tag{7}$$

$$\sigma_0 = \frac{R_e + R_m}{2}, \tag{8}$$

Where $K_{\rho,app}$, $K_{\rho,c}$, $\sigma_{\theta\theta}$, σ_0, R_e and R_m, are respectively: Notch Stress Intensity Factor (NSIF) applied, critical Notch Stress Intensity Factor, hoop stress, reference stress, yield stress, and ultimate strength. It is important to emphasize that the toughness obtained through the intensity NSIF is dependent on notch radius. Having a dimensionless parameter, use the same failure curve wathever the notch radius. The definition of the failure integrity line and the security factor are the same that for the Failure Assessment Diagram. All operating points in the MNFAD are represented by a pair of coordinates (S_r ; $K_{\rho,r}$).

2.3 Fracture toughness in term of $K_{\rho c}$

The fracture toughness depends on notch radius. It is well known that the critical stress intensity factor is proportional to the square root of the notch radius below a critical value ρ_{cr} [7].

$$K_{\rho,c} = \therefore \sqrt{\rho} \quad for\ \rho \geq \rho_{cr}, \tag{9}$$

$$K_{\rho,c} = K_{Ic} \; for \; \rho < \rho_{cr} \,, \tag{10}$$

One notes that fracture toughness measured on specimen with a notch radius greater than ρ_{cr} is denoted $K_{\rho,c}$. This increase of fracture toughness with notch radius is due to the increase of notch plastic zone with notch radius and consequently the increase of total work of fracture. The critical notch radius corresponds to the fact that the notch plastic zone volume is equal to the fracture process zone volume [8]. It appears necessary to measure the fracture toughness with the corresponding gouge radius. In the following, the notch radius $\rho = 0.15$mm is considered as representative of a severe defect and chosen for conservative reasons. This value compared with other obtained from low strength steels is probably below the critical notch radius value. The concept of the critical notch stress intensity factor and corresponding local fracture criterion assume that the fracture process requires a certain fracture process volume [7]. This local fracture approach is called the Volumetric Method. This volume is assumed as a cylinder with a diameter called the effective distance. Determination of the effective distance is based on the bi-logarithmic elastic-plastic stress distribution ahead of the notch because the fracture process zone is the highest stressed zone. This zone is characterized by an inflexion point in the stress distribution at the limit of zones II and zone III in Fig. 4.

$$\sigma_{ef} = \frac{1}{X_{ef}} \int_0^{X_{ef}} \sigma_{yy}(r)\Phi(r)dr \,, \tag{11}$$

Here, σ_{ef}, X_{ef}, $\sigma_{yy}(r)$ and $\Phi(r)$ are effective stress, effective distance, opening stress and weight function, respectively. This stress distribution is corrected by a weight function in order to take into account the distance from notch tip of the acting point and the stress gradient at this point. The effective distance corresponds is to the inflexion point with the minimum of the relative stress gradient χ which can be written as:

$$\chi(r) = \frac{1}{\sigma_{yy}(r)} \frac{\partial \sigma_{yy}(r)}{\partial r} \,, \tag{12}$$

The effective stress is considered as the average value of the stress distribution within the fracture process zone. The notch stress intensity factor is defined as a function of the effective distance and the effective stress [7]:

$$K_\rho = \sigma_{ef} \sqrt{2\pi X_{ef}} \,, \tag{13}$$

and describes the stress distribution in zone III as given by the following equation:

$$\sigma_{yy} = \frac{K_\rho}{(2\pi r)^\alpha} \,, \tag{14}$$

where K_ρ is the notch intensity factor, α is the exponent of the power function of the stress distribution a constant. Failure occurs when the notch stress intensity factor K_ρ reaches the critical value, i.e. the notch fracture toughness $K_{\rho,c}$ which reflects the resistance to fracture initiation from the notch tip. The stress distribution ahead of the notch tip and along notch ligament is computed by Finite Element method for the critical load defined by acoustic emission technique. The critical notch stress intensity factor $K_{\rho,c}$ has been calculated using the effective distance and the effective stress obtained from the relative stress gradient as described in Fig. 5.

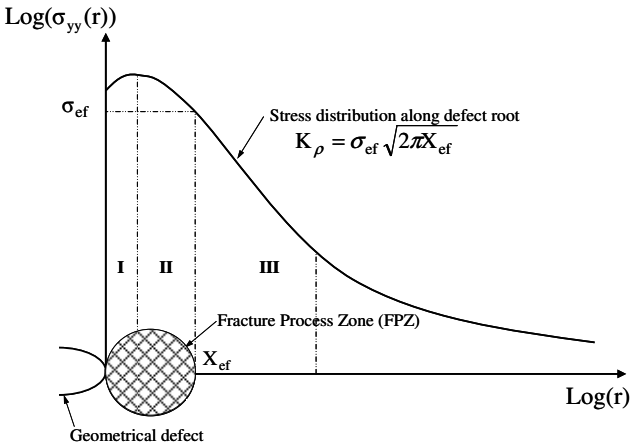

Figure 4. Schematic distribution of elastic-plastic stress ahead of the notch tip on the line of notch extension and the notch stress intensity concept.

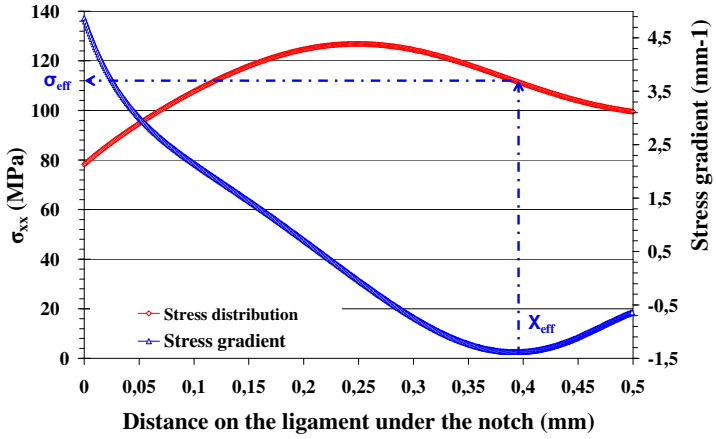

Figure 5. Determination of effective distance using the relative stress gradient method

3.0 TESTS

3.1 Burst tests [9]

Longitudinally notched pipes made in steel API X52 by diameter D=219 mm and wall thickness t=6.1 mm were the object of study, Fig. 6. They were tested for burst under internal pressure, which is presented in Fig. 6. Environmental test conditions: 100% of dry referenced natural gas (methane) and 100% of pure dry hydrogen and free oxygen (less than 1 ppm vol. residual oxygen). To perform tests, a dedicated cell was designed and manufactured. Automatic system for pressure control and test operating according to the assigned sequence was developed [10]. The test cell consists of three cylindrical shells: tube-specimen, external cylinder and internal cylinder. Two lids put down the tube-specimen and external cylinder. A special ring seals provide the compression. The external cylinder (*d= 375 mm*) is needed as a protective housing. The function of the axially aligned internal cylinder (*d= 165 mm*) is to reduce the hydrogen (or hydrogen/natural gas mixture) bulk volume within testing tube. This is necessary because of safety requirements during test procedure.

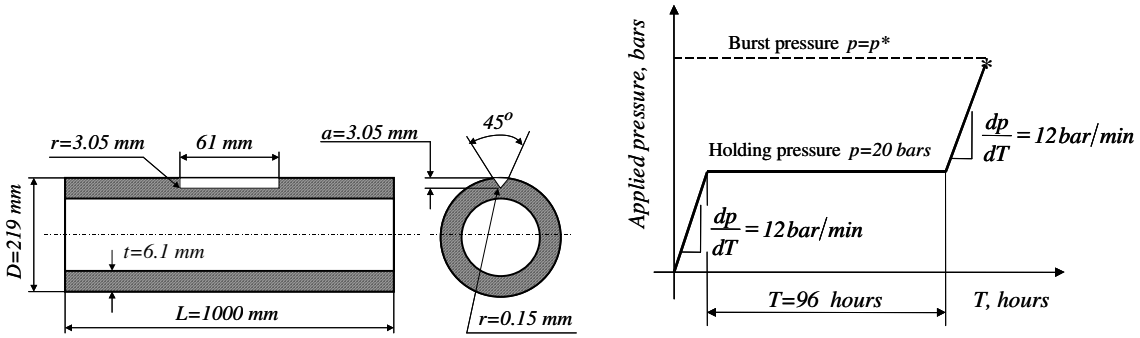

Figure 6. Geometry of the notched pipe and burst cycle

The main objective of the designed cell is creating an additional space, which is filled by inert gas (argon) for avoiding an emergency situation if leakage of hydrogen/natural gas mixture at the pipe burst occurs. The general view of the designed test cell is given in Fig. 7. Here, for pictorial presentation the protective housing is removed. The automatic system for pressure control and test operating according to the assigned sequence is presented in Fig. 7. Tests were carried out in special equipped laboratory with two separate spaces. First room is used for personnel and operating/controlling means. Second room is intrinsically safe space, where the testing stand is located. Gas-cylinders with hydrogen, natural gas, hydrogen/natural gas mixture and argon are boxed outside of the building. Stainless steel gas pipelines are used (internal diameter $d=6$ *mm*, wall thickness $t=2$ *mm*). Before test, all pipelines and cavities of testing cell, cut-off valve and pressure transmitters are purged with argon. The automatic testing system provides the following capabilities:

- Gas pressure transmission in the cavity of testing pipe under assigned rate dp/dT.
- Keeping an assigned internal pressure in testing pipe constant during given time T.
- Loading of the test pipe by internal pressure under given rate dp/dT up to tube burst $p = p^*$.
- Permanent registration of internal pressure $p = \Phi(T)$ in the tube-specimen during test.
- Visualisation of function $p = \Phi(T)$ in real time on the PC monitor for each stage of test.
- Registration and determining of the burst pressure $p = p^*$.
- Permanent registration of pressure on the external tube-specimen surface (space in testing cell that filled by argon) during whole period of test.
- Venting of the test cell (hydrogen/gas mixture + argon) after the tests are finished.
- Safety valve and outlet of the gaseous mixture to atmosphere.

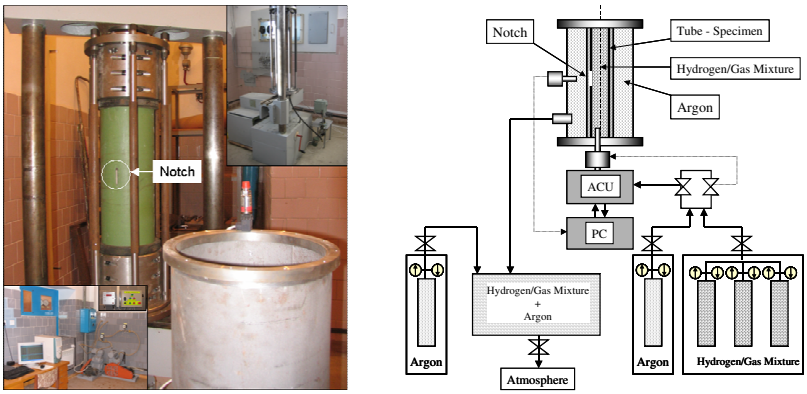

Figure 7. General view of designed testing equipment (protective housing is removed)

3.2 Three points bending tests

For defects assessment of scratches and gouges, it is necessary to determine fracture toughness measured directly on notched specimen [11]. For that we use a non standard specimen, named Roman Tile (RT) specimen, Fig. 8. The advantage of such a specimen geometry is to allow fracture test in radial direction however the low thickness and the important curvature of the pipe.

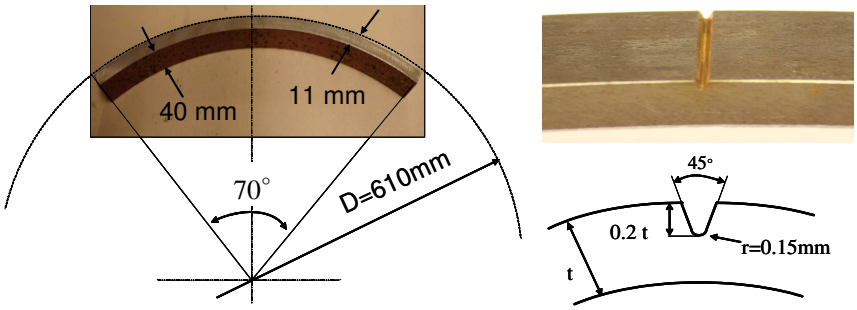

Figure 8. Roman Tile specimen and notch geometry.

The specimen is loaded by three-point bending through a support A and supporting rollers B and C, Fig. 9. Support and rollers were produced from Poly Vinyl Chloride (PVC) to reduce a friction. All was monitored for a constant value of 0.02 mm/s. Test duration was of about 30 minutes.

The V-notch with notch opening angle of 45° and root radius of 0.15 mm was machined to a depth of size a simulating the expected gouge damage. Test specimens have notch aspect ratio $a/W = 0.2$, W corresponding to the wall thickness. A special testing device has been developed for this purpose. The bend-test fixture was positioned on the closed loop hydraulic testing machine with a load cell of capacity ± 10 kN.

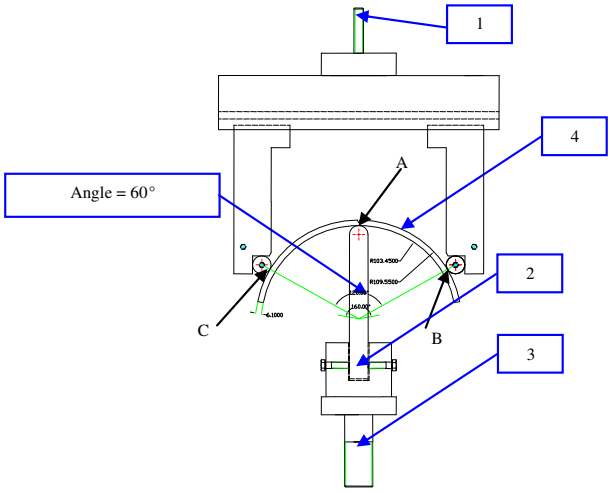

Figure 9. Roman Tile specimen fixture and assembly

1 - connection with load cell;
2 - transmitting component with rounded tip;
3 - connection of test assembly with the testing machine bottom;
4 – "Roman tile" specimen

3.3 Hydrogen electrolytic charging

The study was conducted in a special soil solution NS4 with pH = 6.7, [12]. Chemical composition of this environment is given in Table 3. In these conditions, i.e. in deoxygenated, near-neutral pH solution, the hydrogen atoms are generated on the steel surface by electrochemical reduction of water molecules:

$$H_2O + e \rightarrow H_{ads} + OH^- , \quad (15)$$

The adsorbed hydrogen atoms can subsequently combine into H_2 molecules by the chemical reaction:

$$2H_{ads} \rightarrow H_2 , \quad (16)$$

or the electrochemical reaction:

$$H_{ads} + H_2O + e \rightarrow H_2 + OH^- , \quad (17)$$

Table 3. Chemical composition of NS4 solution (gram/litre), [12]

$NaHCO_3$	KCl	$CaCl_2$	$MgCl_2 \cdot H_2O$
0.483	0.120	0.137	0.131

Here should be noted that, the absorbed hydrogen atom concentration under the cathodic polarisation depends on the hydrogen atom recombination mechanisms. When the chemical reaction Eq. (16) dominates the hydrogen atom recombination, the applied cathodic polarisation enhances the generation of hydrogen atoms and thus the amount of hydrogen atoms penetrating into the steel. The absorbed hydrogen atom concentration will increase continuously with cathodic polarisation potential. In the case of electrochemical reaction Eq. (17), dominating the hydrogen atom recombination, the cathodic polarisation promotes the generation of hydrogen atoms through reaction Eq. (15), and simultaneously, enhances the hydrogen atom recombination through reaction Eq. (17). Thus, the role of cathodic polarisation is to generate hydrogen atoms and also to recombine hydrogen atoms. Accounting the fact that a steady state condition of hydrogen charging cannot be imposed nor obtained in a freely corroding situation, in the presented study the following procedure is made. Specimens were hydrogen charged at constant polarisation potential $E_{cath} = -1000\ mV_{SCE}$, which is slightly more negative for tested steel than free corrosion potential $E_{corr} = -800\ mV_{SCE}$. The specimens were immersed into the cell with special NS4 solution and exposed under constant potential of polarization, E_{cath}. The surface of auxiliary electrode was parallel to notch plane with the distance h = 20 mm.

4.0 RESULTS

4.1 Fracture toughness

Critical load was detected by acoustic emission as for tests in air, and hydrogen condition [11]. The acoustic sensors have been protected against corrosion for tests under hydrogen electrolytic. This critical load is then introduced in a finite Element code to computed notch tip stress distribution. Then effective stress and effective distance are combined through the Volumetric Method to obtain the critical notch stress intensity factor. Finite Element computing is made with the same stress strain curve than for air because:

- there is few difference of the behaviour in air and in presence of hydrogen for small strain,
- the hydrogen affected volume is small compare with the total volume of specimens.

11 tests have been performed with air condition, and 4 with hydrogen electrolytic condition (with 2 different time of exposition, 145 hours and 330 hours). Results are given in the following table:

Table 4. Fracture toughness results in term of $K_{\rho,c}$

	Air	145 hours	330 hours
$K_{\rho,c}(MPa\sqrt{m})$	57.21	47.68	41.78

4.2 Burst pressure

Test results showed that burst pressure for test in methane is equal $p_{\max} = 118\,bar$ and burst pressure for test in hydrogen is equal $p_{\max} = 122 bar$. Therefore, there is no gaseous hydrogen effect on the strength of notched pipes for considered testing conditions.

4.3 Mechanical properties under hydrogen electrolytic

Tensile specimens have been used to characterize mechanical properties of this steel in two environment, air and electrolytic hydrogen. Only a small part of the specimen has been charged under hydrogen, Fig. 10.

The ultimate strength is few affected by hydrogen concentration. However, the elongation at fracture is considerably reduced as can be seen on Table 5.

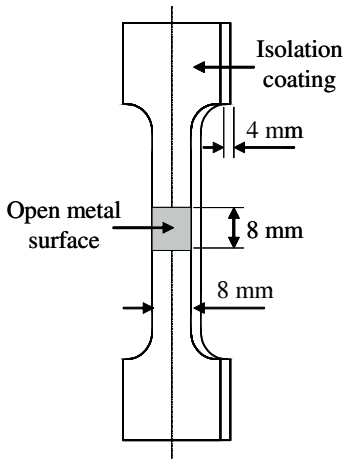

Figure 10. Specimen used to the hydrogen charging.

Table 5. Influence of hydrogen concentration on tensile properties of X52 steel.

	Yield stress (MPa)	Ultimate strength (MPa)	Elongation at fracture (%)
Air	453	524	14.03
Hydrogen	479	547	11.44

4.4 Security and safety factors

The MNFAD is then applied using the data reported in tables 6 and 7.

Table 6. Obtained values of effective distance, effective stress, notch stress intensity factor and hoop stress for conditions described.

σ_{ef} (MPa$\sqrt{m}$)	X_{ef} (mm)	K_ρ (MPa$\sqrt{m}$)	$\sigma_{\theta\theta}$ (MPa)
343	0.67	15.8	125

Table 7. Average of materials properties with and without hydrogen; calculated values of parameters k_r and S_r.

	$K_{\square,c}$ (MPa$\sqrt{m}$)	$\sigma_0 = \sigma_u + \sigma_y / 2$ (MPa)	$k_r = K_\rho / K_{\rho,c}$	$S_r = \sigma_{\theta\theta} / \sigma_0$
Air	57.21	496	0.276	0.252
Hydrogen	44.73	513	0.35	0.244

The safety factor for the same defect and for the same service conditions , one for material without hydrogen embrittlement, the second with hydrogen embrittlement are then established. The corresponding values are reported in Fig. 11. One notes that hydrogen embrittlement leads to a reduction of the safety factor of 18.33%.

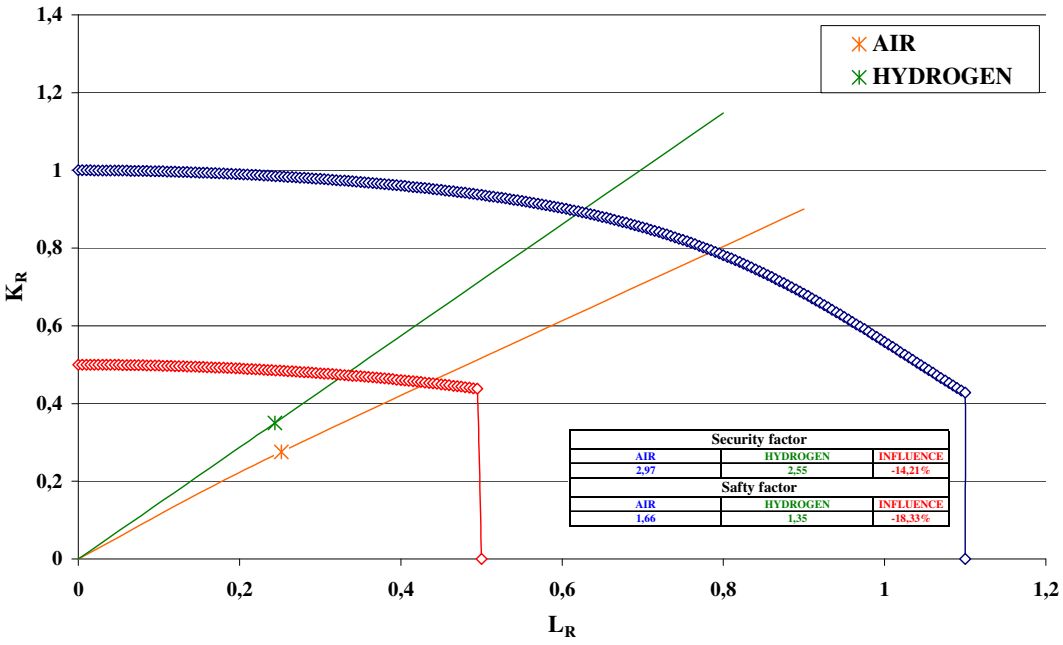

Figure 11. Specimen used to the hydrogen charging.

In hydrogen condition, the security factor is decreased by 14%, but its value is always over the conventional value of 2. The safety factor is somewhat more affected, 18%. In severe conditions, hydrogen electrolytic, the decreasing of the different factor, is so acceptable.

5.0 CONCLUSIONS

To assess nocivity of a pipe surface defect such as gouge, a modified Failure Assessment (MNFAD) as been established based on Volumetric Method (VM) of the notch fracture Mechanics. This MNFAD is coupled with the SINTAP failure curve and allows determining the safety factor associated with defect geometry, loading conditions and material resistance. Determination of the assessment point needs to determine fracture toughness in radial direction of low thickness and high curvature pipe. This has been done using a special specimen, the Roman Tile. Tensile properties have been measured in electrolytic hydrogen charging method. The obtained data coupled with the MNFAD method lead to the conclusion that in presence of a severe surface gouge defect, the reduction of the safety factor is 14 % but remains over the conventional value of 2. These results indicate the possibility to use the actual existing European natural gas pipe network for the transport of a mixture of natural gas and hydrogen.

REFERENCES

1. Fernandes T. R. C., da Graça Carvalho F. C. and M., "HySociety" in support of European hydrogen projects and EC policy. International Journal of Hydrogen Energy, 30 (2005) 239-245
2. Mulder G., Hetland J. and Lenaers G. Towards a sustainable hydrogen economy: Hydrogen pathways and infrastructure. International Journal of Hydrogen Energy, 32, Issues 10-11 (2007) 1324-1331
3. NaturalHy Project, *http://www.naturalhy.net*
4. Rapport de l'enquête MH-2-95, "Fissuration par corrosion sous tension des oléoducs et des gazoducs canadiens", Office National d'Energie, (1996)
5. J. Capelle, I. Dmytrakh, J. Gilgert, Ph. Jodin, G. Pluvinage, "A comparison of experimental results and computations for cracked tubes subjected to internal pressure", Materials and Technology 40, 233-237, (2006)
6. SINTAP: Structural Integrity Assessment Procedure, Final Report E-U project BE95-1462 Brite Euram Programme Brussels (1999).
7. G Pluvinage "Fracture and Fatigue emanating from stress concentrators"; Kluwer, (2003).
8. Akourri O, Louah M, Kifani A, Gilgert G, Pluvinage G., "The effect of notch radius on fracture toughness J_{IC} ", Eng Fract Mech 65, pp 491-505, (2000)
9. J. Capelle, J. Gilgert, I. Dmytrakh, G. Pluvinage, "Sensitivity of pipelines with steel API X52 to hydrogen embrittlement", International Journal of Hydrogen Energy 33, issue 24, pp 7630-7641, (2008)
10. Burst tests on pipes under pressure of mixture of hydrogen and natural gas. Final report on Subcontract No 1401-2005 of NATURALHY-Project (Contract No SES6/2004/502661). Karpenko Physico-Mechanical Institute of National Academy of Sciences of Ukraine, Lviv, Ukraine (2006).
11. J. Capelle, J. Gilgert, I. Dmytrakh, G. Pluvinage, "Hydrogen effect on fatigue and fracture resistance of a pipe steel", Structural Integrity and Life, volume 9, n° 1, pp. 9–14, (2009)
12. J. Capelle, I. Dmytrakh, G. Pluvinage, "Electrochemical Hydrogen Absorption of API X52 Steel and its Effect on Local Fracture Emanating from Notches", Structural Integrity and Life, volume 9, n° 1, pp. 3–8, (2009)